Inorg. Chem. **2006**, *45*, 5501–5509

Comparison of the Crystal Structures and Magnetic Properties of the Low- and High-Temperature Forms of $AgCuPO_4$: Crystal Structure Determination, Magnetic Susceptibility Measurements, and Spin Dimer Analysis

Hamdi Ben Yahia, Etienne Gaudin, and Jacques Darriet*

Institut de Chimie de la Matière Condensée de Bordeaux (ICMCB−CNRS), Université de Bordeaux 1, 87 Avenue du Docteur A. Schweitzer, 33608 Pessac Cedex, France

Dadi Dai and Myung-Hwan Whangbo*

Department of Chemistry, North Carolina State University, Raleigh, North Carolina 27695-8204

Received March 22, 2006

The crystal structure of the low-temperature form of $AgCuPO_4$ (i.e., α-$AgCuPO_4$) was determined by powder X-ray diffraction and was compared with that of the high-temperature form of $AgCuPO_4$ (i.e., β-$AgCuPO_4$). The magnetic properties of the two forms were examined by measuring their magnetic susceptibilities and evaluating the relative strengths of their spin-exchange interactions on the basis of spin-dimer analysis. Both forms of $AgCuPO_4$ have layers of $Cu_2P_2O_8$ alternating with silver-atom double layers; β-$AgCuPO_4$ has two $Cu_2P_2O_8$ layers per unit cell, while α-$AgCuPO_4$ has one. The coordinate environment of each Cu^{2+} ion is close to being a distorted square pyramid in α-$AgCuPO_4$, but it is close to being a distorted trigonal bipyramid in β-$AgCuPO_4$. The magnetic susceptibilities of α- and β-$AgCuPO_4$ are well simulated by an antiferromagnetic alternating-chain model, which leads to $J/k_B = -146.1$ K and $\alpha J/k_B = -75.8$ K for α-$AgCuPO_4$, and $J/k_B = -82.6$ K and $\alpha J/k_B = -31.7$ K for β-$AgCuPO_4$ (with the convention in which the spin-exchange parameter between two adjacent spin sites is written as $2J$). The spin gaps, Δ/k_B, obtained from these parameters are 93.7 K for α-$AgCuPO_4$ and 62.3 K for β-$AgCuPO_4$. The strongest spin exchange in both forms of $AgCuPO_4$ comes from a super-superexchange path, and this interaction is stronger for α-$AgCuPO_4$ than for β-$AgCuPO_4$ by a factor of $\sim$2, in good agreement with the experiment. Our analysis supports the use of this model for β-$AgCuPO_4$ and indicates that the spin lattice of α-$AgCuPO_4$ would be better described by a two-dimensional net made up of weakly interacting alternating chains.

1. Introduction

There have been a number of studies on compounds of the formula $AMPO_4$, where A is an alkali atom or Ag and M is a transition metal. The crystal structures of $AMPO_4$ depend strongly on the size of the monovalent A^+ cation. With A = Li, the $AMPO_4$ compounds adopt the olivine-type structure. Since the study of its electrochemical properties by Goodenough et al.,[1] $LiFePO_4$ has been extensively studied among the olivine series $LiMPO_4$. Several studies have shown that $LiFePO_4$ is a promising high-potential cathode material for rechargeable Li-ion batteries.[2,3] With A = Na, the $AMPO_4$ compounds have the maricite-type structure. In the case of $NaCuPO_4$, two structural phases are found: the high-temperature form, β-$NaCuPO_4$, has the maricite-type structure;[4,5] the low-temperature form, α-$NaCuPO_4$, has a zeolite-ABW structure,[6] and the two forms undergo a reversible phase transition at 957 K.[6] A larger

* To whom correspondence should be addressed. E-mail: mike_whangbo@ncsu.edu (M.-H.W.); darriet@icmb-bordeaux.cnrs.fr (J.D.).

(1) Pahdi, A. K.; Nanjundaswamy, K. S.; Goodenough, J. B. *J. Electrochem. Soc.* **1997**, *144*, 1188.
(2) Chung, S.-Y.; Bloking, J. T.; Chiang, Y.-M. *Nature Mater.* **2002**, *1*, 123.
(3) Herle, P. S.; Ellis, B.; Coombs, N.; Nazar, L. F. *Nature Mater.* **2004**, *3*, 147.
(4) Quarton, M.; Oumba, M. T.; Kolsi, A. W. *J. Appl. Crystallogr.* **1983**, *16*, 576.
(5) Kawahara, A.; Kageyama, T.; Watanabe, I.; Yamakawa, J. *Acta Crystallogr.* **1993**, *C49*, 1275.
(6) Quarton, M.; Kolsi, A. W. *Acta Crystallogr.* **1983**, *C39*, 664.

10.1021/ic060484l CCC: $33.50
Published on Web 06/07/2006

alkali cation leads to structures with an open framework derived from the stuffed-tridymite or zeolite-ABW structure type.[7] When A^+ is a d^{10} cation, Ag^+, other structural types of $AMPO_4$ are found as observed for $AgCoPO_4$[8] and $AgCuPO_4$.[9] There are two structural forms of $AgCuPO_4$ (i.e., the high-temperature form, β-$AgCuPO_4$, and the low-temperature form, α-$AgCuPO_4$),[9] and an irreversible phase transition from the α- to the β-form takes place at 848 K.[9] The crystal structure of β-$AgCuPO_4$ is known, but that of α-$AgCuPO_4$ has not been reported so far.

In the present work, we determine the crystal structure of α-$AgCuPO_4$ by X-ray powder diffraction and compare the crystal structures of α-$AgCuPO_4$ and β-$AgCuPO_4$. Then, we measure the temperature-dependent magnetic susceptibilities of both forms of $AgCuPO_4$ and examine how the subtle difference in their crystal structures is manifested in their magnetic properties. Finally, we perform spin-dimer analysis to evaluate the relative strengths of the various spin-exchange interactions in α- and β-$AgCuPO_4$ and identify the spin lattices relevant for describing their magnetic properties.

2. Experimental Section

α-$AgCuPO_4$ was prepared by standard solid-state reactions, using high purity Ag_2O (99.99%, Aldrich), CuO (99%, Aldrich), and $(NH_4)H_2PO_4$ (99.99%, Aldrich) as starting materials. After it was fired at 450 °C for 24 h in an oxygen atmosphere, the mixture was ground, pelletized, and heated at 530 °C for 100 h with intermediate grindings to ensure a total reaction. The progress of the reaction was monitored by X-ray powder diffraction. As observed previously,[9] α-$AgCuPO_4$ transforms irreversibly to β-$AgCuPO_4$ at 848 K. This transition is accompanied by a change in color from green to yellow green. Diffraction data suitable for structure analysis of α-$AgCuPO_4$ were collected using a Philips X-pert diffractometer operating in Bragg−Brentano geometry with Cu Kα1 radiation. Data were collected over the angular range of $5 \leq 2\theta \leq 120°$ with $\Delta(2\theta) = 0.02°$. Dicvol[10] was used for the determination of the unit cell parameters. The X-ray diffraction data were analyzed by a Le Bail profile analysis[11] and refined by the Rietveld method as implemented in the JANA2000 program suite.[12] The background was estimated by a Legendre polynomial, and the peak shapes were described by a pseudo-Voigt function varying five profile coefficients.[13]

The magnetic susceptibilities of α-$AgCuPO_4$ and β-$AgCuPO_4$ were measured over the temperature range of $5 \leq T \leq 340$ K using a Quantum Design MPMS-5 SQUID magnetometer. Data were collected during the warm-up at 0.5 T, after the sample was cooled in zero applied field. Diamagnetic corrections were carried out on the basis of Pascal's tables.

(7) Meier, W. M.; Olson, D. H.; Baerlocher, Ch. *Atlas of Zeolite Structure Types* ; Elsevier: Amsterdam, 1996.
(8) Tordjman, I.; Guitel, J. C.; Durif, A.; Averbuch, M. T.; Masse, R. *Mater. Res. Bull.* **1978**, *13*, 983.
(9) Quarton, M.; Oumba, M. T. *Mater. Res. Bull.* **1983**, *18*, 967.
(10) Boultif, A.; Louer, D. *J. Appl. Crystallogr.* **2004**, *37*, 724.
(11) Le Bail, A.; Duroy, H.; Fourquet, J. L. *Mater. Res. Bull.* **1988**, *23*, 447.
(12) Petricek, V.; Dusek, M., *The Crystallographic Computing System Jana*; Institute of Physics: Praha, Czech Republic, 2000.
(13) Thompson, P.; Cox, D. E.; Hastings, J. B. *J. Appl. Crystallogr.* **1987**, *20*, 79.

Table 1. Atomic Coordinates and Isotropic Displacement Parameters of α-$AgCuPO_4$[a]

atoms	occupancy	site	*x*	*y*	*z*	U_{iso} (Å^2)
Ag	1	4e	0.9287(4)	0.1093(6)	0.1909(5)	0.0302(11)[b]
Cu	1	4e	0.5834(13)	0.120(2)	0.8533(15)	0.024(3)
P	1	4e	0.2752(6)	0.1144(12)	0.4924(7)	0.0231(18)
O1	1	4e	0.315(3)	0.951(4)	0.649(3)	0.031(8)
O2	1	4e	0.276(2)	0.986(3)	0.312(3)	0.012(7)
O3	1	4e	0.099(3)	0.237(4)	0.492(3)	0.023(7)
O4	1	4e	0.428(3)	0.305(4)	0.520(3)	0.029(8)

[a] Space group = $P2_1/c$, $Z = 4$, $a = 7.83650(10)$ Å, $b = 5.62685(7)$ Å, $c = 7.49381(10)$ Å, $\beta = 99.0673(11)°$, $R_{Bragg} = 4.75\%$, $R_p = 9.53\%$, $R_{wp} = 12.80\%$, $\chi^2 = 2.48$. [b] The anisotropic displacement parameters of Ag are as follows: $U_{11} = 0.0205(17)$, $U_{22} = 0.0310(18)$, $U_{33} = 0.040(2)$, $U_{12} = 0.000(2)$, $U_{13} = 0.0091(15)$, and $U_{23} = -0.001(2)$.

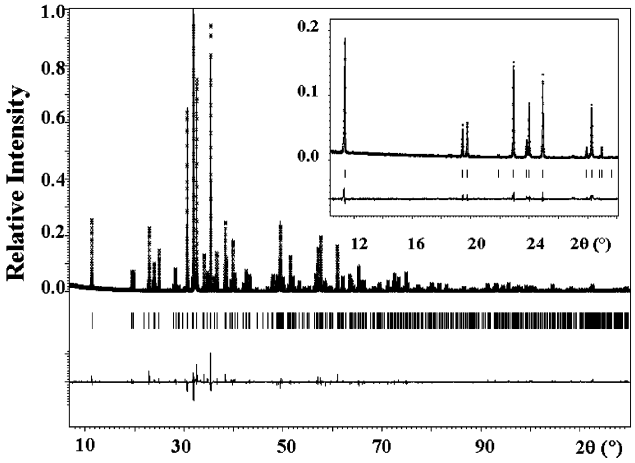

Figure 1. Observed (cross), calculated (solid line), and difference (bottom) X-ray powder diffraction patterns for α-$AgCuPO_4$. The inset shows a zoom-in view of the low-angle region of the diffractogram.

3. Crystal Structure of the Low-Temperature Form, α-$AgCuPO_4$

All of the diffraction peaks of α-$AgCuPO_4$ were indexed by a monoclinic unit cell with lattice parameters of $a = 7.83650(10)$ Å, $b = 5.62685(7)$ Å, $c = 7.49381(10)$ Å, and $\beta = 99.0673(11)°$. A possible space group compatible with the index of the Bragg peaks was found to be $P2_1/c$. The structure was solved from the Patterson map. In the first step, the positions of the two heaviest atoms, silver and copper, were deduced. The first refinements confirmed the space group $P2_1/c$. It was straightforward to deduce the atomic positions of the phosphorus and four oxygen positions from the difference Fourier map. Refinement results are given in Table 1, and the profile fit is shown in Figure 1. All the atoms occupy the 4e general site with full occupancy. Selected interatomic distances and angles are listed in Table 2. Isotropic atomic displacement parameters (ADPs) were used for all atomic positions except for Ag, for which it was possible to introduce anisotropic ADPs. The crystallographic data are given in the Supporting Information.

A projection view of the structure of α-$AgCuPO_4$ along the *b* direction is given in Figure 2a. The structure consists of $Cu_2P_2O_8$ layers parallel to the (100) plane, which are separated by silver double layers. The local environment of Cu^{2+} is a distorted square pyramid with four Cu to basal O

Table 2. Selected Bond Lengths (Å), Bond Valences, and Bond Angles (deg) of α-$AgCuPO_4$

distances		bond valence [a]	angles	
Cu−O1′	2.58(2)	0.088	O1−Cu−O1′	128.3(9)
Cu−O1	2.03(2)	0.387	O1′-Cu−O2	90.1(8)
Cu−O2	1.88(2)	0.581	O1−Cu−O2	90.8(9)
Cu−O4	2.02(2)	0.398	O1′-Cu−O4	82.2(9)
Cu−O4′	1.92(3)	0.521	O1′-Cu−O4′	85.9(9)
		sum = 1.98	O1−Cu−O4′	95.4(11)
P−O1	1.48(2)	1.398	O2−Cu−O4	96.0(10)
P−O2	1.53(2)	1.221	O4−Cu−O4′	78.9(10)
P−O3	1.54(3)	1.189	Cu−O4−Cu	101.1(10)
P−O4	1.60(2)	1.011		
		sum = 4.82	O1−P−O2	112.2(12)
Ag−O1	2.43(3)	0.185	O1−P−O3	110.8(13)
Ag−O2	2.66(2)	0.099	O1−P−O4	104.7(12)
Ag−O3	2.54(2)	0.137	O2−P−O3	109.7(10)
Ag−O3	2.49(2)	0.157	O2−P−O4	108.8(11)
Ag−O3	2.32(2)	0.249	O3−P−O4	110.5(12)
		sum = 0.82		

[a] Bond valence = $e^{(r_0-r)/b}$ with the following parameters:[31] $b = 0.37$, $r_0 = 1.679$ for Cu−O, $r_0 = 1.604$ for P−O, and $r_0 = 1.805$ for Ag−O.

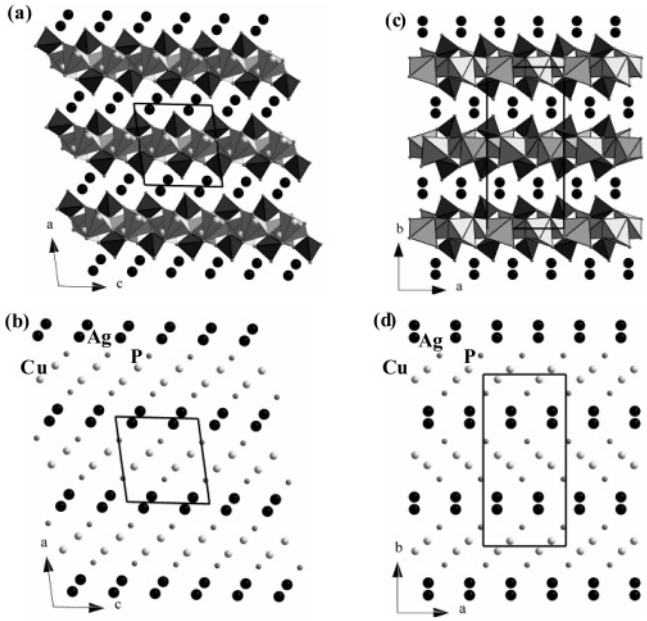

Figure 2. Schematic drawings that represent the crystal structures of α-$AgCuPO_4$ and β-$AgCuPO_4$: (a) projection view of the structure of α-$AgCuPO_4$ along the *b* direction, (b) projection view of the Cu, P, and Ag atom arrangement along the *b* direction, (c) projection view of the structure of β-$AgCuPO_4$ along the *c* direction, and (d) projection view of the Cu, P and Ag atom arrangement along the *c* direction.

atom ($Cu-O_{ba}$) distances in the range of 1.88−2.03 Å and a Cu to apical O atom ($Cu-O_{ap}$) distance of 2.58 Å (Figure 3a, Table 2). The average of the four $Cu-O_{ba}$ distances is 1.96 Å, which is close to the ionic radii sum.[14] The bond valence sum [15] for Cu is calculated to be 1.98, in good agreement with the +2 oxidation state expected for Cu. Every two CuO_5 distorted square pyramids share one common basal edge to form a Cu_2O_8 dimer (Figure 3a) with a Cu−Cu distance of 3.05 Å and the Cu−O−Cu bridging angle of 101.1°. The Cu_2O_8 dimers are corner-shared with PO_4 tetrahedra to form $Cu_2P_2O_8$ layers parallel to the (100) plane (Figure 2a). A perspective view of a single $Cu_2P_2O_8$ layer is presented in Figure 4a, where every two nearest-neighbor Cu atoms are connected either by two Cu−O−Cu bridges, as in the Cu_2O_8 dimers, or by one Cu−O−Cu bridge. A simplified view of a $Cu_2P_2O_8$ layer showing only the Cu atoms is shown in Figure 4b, where each linkage between adjacent Cu atoms is represented by a cylinder. Each Cu−Cu linkage with two Cu−O−Cu bridges is indicated by a blue cylinder, and that with one Cu−O−Cu bridge is represented by an aquamarine cylinder. In successive $Cu_2P_2O_8$ layers of α-$AgCuPO_4$, the orientation of the Cu and P atom arrangement is identical, as depicted in Figure 2b.

The silver atom is surrounded by five oxygen atoms with Ag−O distances ranging between 2.32 and 2.66 Å, in good agreement with those observed in β-$AgCuPO_4$.[9] The bond valence sum for Ag is calculated to be 0.82, confirming the oxidation state of +1 for Ag. The local environment of Ag^+ is a distorted trigonal bipyramid, which is axially compressed along the pseudo-3-fold rotational axis with the average Ag to axial O distance of 2.38 Å and an average Ag to equatorial O distance of 2.56 Å (Table 2).

4. Comparison of the Crystal Structures of the High- and Low-Temperature Forms of $AgCuPO_4$

The high-temperature form β-$AgCuPO_4$ consists of $Cu_2P_2O_8$ layers parallel to the (010) plane, which alternate with double layers of silver atoms (Figure 2c). β-$AgCuPO_4$ crystallizes with orthorhombic symmetry (space group = *Pbca*, $Z = 8$) with $a = 7.500(1)$ Å, $b = 15.751(2)$ Å, and $c = 5.702(1)$ Å.[9] The *c* and *a* parameters of the high-temperature form are comparable in value to the *b* and *c* parameters, respectively, of the low-temperature form. Moreover, the *b* parameter of the high-temperature form is very close to being twice the *a* parameter of the low-temperature form (Table 1). This is readily understood by considering the repeat patterns of the Cu and P atoms in successive $Cu_2P_2O_8$ layers. In the low-temperature form, the orientation of the Cu and P atom arrangement is parallel to the [101] direction (Figure 2b), so that there is one $Cu_2P_2O_8$ layer per unit cell. In the high-temperature form, the orientation of the Cu and P atom arrangement is parallel to the [110] direction in one layer and to the $[1\bar{1}0]$ direction in the adjacent layers, so that there are two $Cu_2P_2O_8$ layers per unit cell (Figure 2d). Thus, the high-temperature form has an antiphase boundary (APB) without composition change. The APB plane is perpendicular to the *b* direction (Figure 2d). One consequence of the APB in the high-temperature form and its absence in the low-temperature form is that the local coordination environment of Cu^{2+} is close to being a distorted square pyramid in the low-temperature form (Figure 3a), while it is close to being a distorted trigonal bipyramid in the high-temperature form (Figure 3b). The trigonal bipyramid is compressed along the pseudo-3-fold rotational axis (i.e., the O3−O2′ direction). Two CuO_5 trigonal bipyramids share the O2′−O2 edge to form an isolated dimer (Figure 3b), and these dimers are linked by the PO_4 tetrahedra leading to the $Cu_2P_2O_8$ layers. Although it was not shown for lack of space, a single $Cu_2P_2O_8$ layer of β-$AgCuPO_4$ has the structure similar to

(14) Shannon, R. D. *Acta Crystallogr.* **1976**, *A32*, 751.
(15) Brown, I. D.; Altermatt, D. *Acta Crystallogr.* **1985**, *B41*, 244.

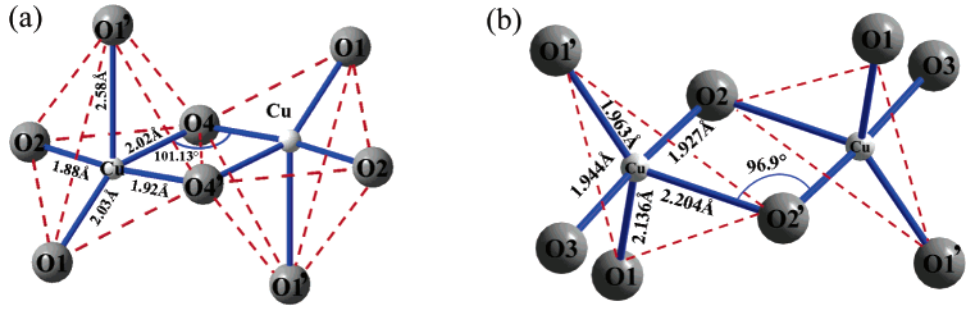

Figure 3. Edge-sharing dimers Cu_2O_6 of (a) α-$AgCuPO_4$ and (b) β-$AgCuPO_4$

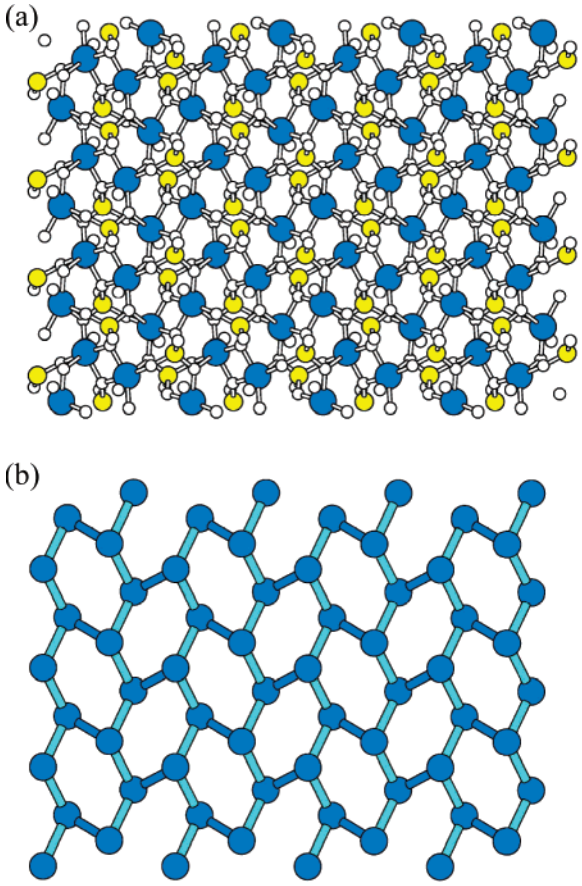

Figure 4. Schematic drawings showing the structure of a single $Cu_2P_2O_8$ layer of α-$AgCuPO_4$. (a) Ball-and-stick view of the Cu, P, and O atoms along the *c* direction, where the blue, yellow, and white circles represent the Cu, P, and O atoms, respectively. (b) Ball-and-stick view of only the Cu atoms along the *c* direction. Each blue cylinder represents a pair of nearest-neighbor Cu atoms linked by two Cu−O−Cu linkages, and each aquamarine cylinder respresents a pair linked by one Cu−O−Cu linkage.

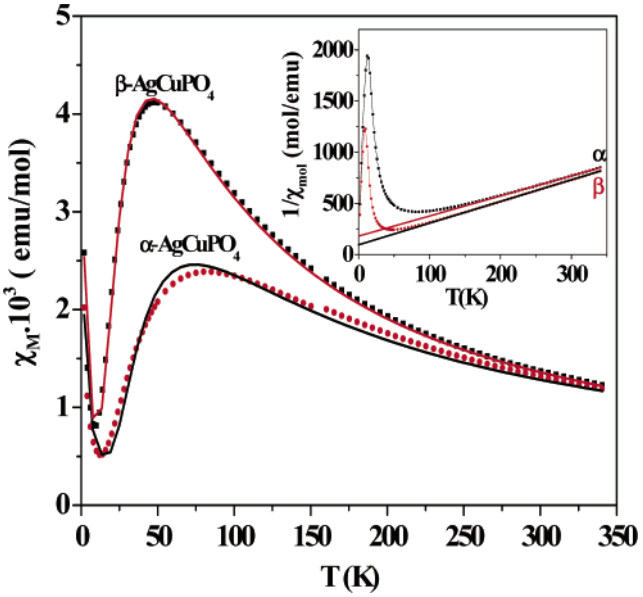

Figure 5. Magnetic susceptibilities of α-$AgCuPO_4$ and β-$AgCuPO_4$ as a function of temperature. The experimental points are represented by filled black squares for β-$AgCuPO_4$ and filled red circles for α-$AgCuPO_4$. The solid lines represent the calculated values using a dimer model. The inset displays the reciprocal magnetic susceptibilities as a function of temperature.

that presented in Figure 4 for a single $Cu_2P_2O_8$ layer of α-$AgCuPO_4$.

5. Magnetic Susceptibility and Fitting Analysis

There is no previous study of magnetic susceptibility on α-$AgCuPO_4$. There is one study of magnetic susceptibility on β-$AgCuPO_4$,[9] but it did not report the temperature dependence of the magnetic susceptibility. The magnetic susceptibility versus temperature (χ vs T) plots for α- and β-$AgCuPO_4$ are presented in Figure 5, and the corresponding χ^{-1} versus T plots are shown in the inset. In the temperature range of 100−340 K, the susceptibilities of the two structures follow a Curie−Weiss law with negative Weiss temperatures, thereby indicating predominantly antiferromagnetic interactions between adjacent Cu^{2+} ions. The paramagnetic regions of the χ versus T plots of α- and β-$AgCuPO_4$ (i.e., above 200 and 150 K, respectively) were least-squares fitted in terms of a Curie−Weiss susceptibility, $C/(T - \theta)$, plus a weak temperature-independent paramagnetism, χ_{tip}. This fitting analysis leads to $C = 0.46$ mol^{-1} cm^3 K, $\theta = -76(1)$ K, and $\chi_{tip} = 8 \times 10^{-5}$ cm^3 mol^{-1} for α-$AgCuPO_4$ and $C = 0.45$ mol^{-1} cm^3 K, $\theta = -38(1)$ K, and $\chi_{tip} = 4 \times 10^{-5}$ cm^3 mol^{-1} for β-$AgCuPO_4$. The effective magnetic moments, μ_{eff}, calculated from the Curie constants, C, are 1.92 and 1.90 μ_B for α-$AgCuPO_4$ and β-$AgCuPO_4$, respectively. These values are consistent with the fact that the effective magnetic moment, μ_{eff}, should be greater than the spin-only value (1.73 μ_B) because the g factor of Cu^{2+} is greater than 2.

The magnetic susceptibilities of α-$AgCuPO_4$ and β-$AgCuPO_4$ exhibit a maximum at $T_{max} = \sim 75$ and ~ 50 K, respectively, and they show a local minimum at $T_{min} = \sim 25$ and ~ 10 K, respectively. The magnetic susceptibilities show a small increase below T_{min}. For both forms of $AgCuPO_4$,

the shape of their magnetic susceptibilities clearly show that they have a spin gap (i.e., an energy gap in the magnetic energy spectrum from the singlet ground state to the first excited state). The small susceptibility increase below T_{min} is attributed to the contribution of a magnetic impurity, which follows a Curie−Weiss law. To gain insight into the spin-gapped behavior of α- and β-$AgCuPO_4$, it is necessary to identify spin lattice models that simulate their magnetic susceptibilities. A spin gap is found for several spin lattices, and the archetypal systems are an antiferromagnetic dimer and an antiferromagnetic alternating chain. It is of interest if these two models can describe the magnetic susceptibilities of α- and β-$AgCuPO_4$.

The spin Hamiltonian of a dimer is written as

$$\hat{H}_{dimer} = -2J\hat{S}_1\hat{S}_2 \quad (1)$$

and that of an alternating chain (a-chain) as

$$\hat{H}_{a-chain} = -2\sum_n (J\hat{S}_{2n-1}\hat{S}_{2n} + \alpha J\hat{S}_{2n}\hat{S}_{2n+1}) \quad (2)$$

An isolated dimer is described by one spin-exchange parameter, J, and an alternating chain is described by two spin exchange parameters, J and αJ ($0 < \alpha < 1$). The Van Vleck magnetic susceptibilities expected from these spin Hamiltonians are given by[16,17]

$$\chi_{dimer} = \frac{N\beta^2 g^2}{k_B T}\frac{2\exp(2x)}{1+3\exp(2x)} \quad (3)$$

$$\chi_{a-chain} = \frac{N\beta^2 g^2}{k_B T}\frac{A+Bx+Cx^2}{1+Dx+Ex^2+Fx^3} \quad (4)$$

where $x = |J/k_BT|$. Coefficients $A-F$ of eq 4 are functions of α; there is one set of $A-F$ values for $\alpha \geq 0.4$ and another set for $\alpha \leq 0.4$.[17] Equation 4 is known to be valid for temperatures, T, greater than $0.5|J|/k_B$.[17] Johnston et al.[18] reported a more accurate magnetic susceptibility expression for an alternating Heisenberg chain that covers a wider temperature range and is valid for all α values; it is not reproduced here because of its complexity. We simulate the experimental magnetic susceptibility, χ_{exp}, with the following expression

$$\chi_t = (1-x)\chi_{theoret} + x\frac{C}{T-\theta} + \chi_{tip} \quad (5)$$

In case of weak interactions between the magnetic entities (i.e., dimers in a dimer model and alternating chains in an alternating chain model), $\chi_{theoret} = \chi_{dimer}$ for a dimer model and $\chi_{theoret} = \chi_{a-chain}$ for an alternating chain model. The second term of eq 5 is a Curie−Weiss term $C/(T-\theta)$ for the magnetic impurity with x representing the mole fraction of the impurity. The last term χ_{tip} is the temperature-independent term. If the interactions between the adjacent magnetic entities are included under the mean-field approximation,[19] $\chi_{theoret}$ is written as

$$\chi_{theoret} = \frac{\chi}{1-(zJ'/N\beta^2 g^2)\chi} \quad (6)$$

where $\chi = \chi_{dimer}$ for a dimer model, and $\chi = \chi_{a-chain}$ for an alternating chain model. The parameter zJ' measures how strongly the adjacent magnetic entities interact, but it should be noted that eq 6 is valid only when the zJ'/J ratio is not greater than 0.1 in magnitude.

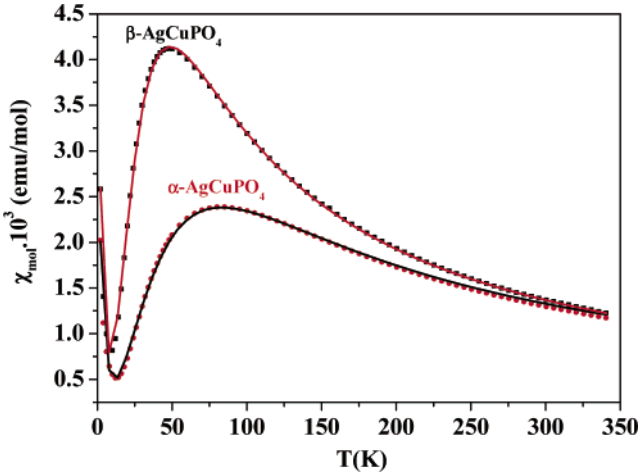

Figure 6. Magnetic susceptibilities of α-$AgCuPO_4$ and β-$AgCuPO_4$ as a function of temperature. The experimental points are represented by filled black squares for β-$AgCuPO_4$ and filled red circles for α-$AgCuPO_4$. The solid lines represent the calculated values using an alternating chain model.

A least-squares fitting of χ_{exp} with χ_t using a dimer model was not successful if the interdimer interactions are neglected (hence not shown). Once the latter are included, the experimental susceptibility can be well simulated, as shown by the solid lines in Figure 5. The fitting parameters for α-$AgCuPO_4$ are $J/k_B = -61.1(5)$ K, $zJ'/k_B = -45(2)$ K, $x = 0.017(1)$, $C = 0.4$ cm^3 mol^{-1} K, $g = 2.215$, $\theta = -0.94(1)$ K, and $\chi_{tip} = 8 \times 10^{-5}$ cm^3 mol^{-1}, while those for β-$AgCuPO_4$ are $J/k_B = -38.1(1)$ K, $zJ'/k_B = -15.4(5)$ K, $x = 0.019(1)$, $C = 0.4$ cm^3 mol^{-1} K, $g = 2.18$, and $\chi_{tip} = 4 \times 10^{-5}$ cm^3 mol^{-1}. Although the fitting is reasonably good, the zJ'/J ratio required for the fitting is too large to be meaningful (i.e., 0.74 for α-$AgCuPO_4$ and 0.41 for β-$AgCuPO_4$). Consequently, an isolated dimer model is not appropriate for both α- and β-$AgCuPO_4$.

A least-squares fitting of χ_{exp} using an alternating chain model with the expression of χ_t given by Hall et al.[17] was successful even without including the interchain interactions, as shown by the solid lines in Figure 6. The fitting parameters for α-$AgCuPO_4$ are $J/k_B = -146.1(3)$ K, $\alpha = 0.519(3)$, $g = 2.215$, $C = 0.4$ cm^3 mol^{-1} K, $\theta = -3.26(7)$ K, $x = 0.045(1)$, and $\chi_{tip} = 8 \times 10^{-5}$ cm^3 mol^{-1}, while those for β-$AgCuPO_4$ are $J/k_B = -82.6(1)$ K, $\alpha = 0.384(3)$, $g = 2.18$, $C = 0.4$ cm^3 mol^{-1} K, $\theta = -1.74(6)$ K, $x = 0.032(1)$, and $\chi_{tip} = 4 \times 10^{-5}$ cm^3 mol^{-1}. Thus, an alternating chain model using the expression of χ_t given by Hall et al.[17] provides a

(16) Bleany, B.; Bowers, K. D. *Proc. R. Soc. London, Ser. A* **1952**, *214*, 451.
(17) Hall, J. W.; Marsh, W. E.; Weller, R. R.; Hatfield, W. E. *Inorg. Chem.* **1981**, *20*, 1033.
(18) Johnston, D. C.; Kremer, R. K.; Troyer, M.; Wang, X.; Klümper, A.; Bud'ko, S. L.; Panchula, A. F.; Canfield, P. C. *Phys. Rev. B* **2000**, *61*, 9558.
(19) Ginsberg, A. P.; Lines, M. E. *Inorg. Chem.* **1972**, *11*, 2289.

reasonable description of the temperature-dependence of the magnetic susceptibility for both α- and β-$AgCuPO_4$, although eq 4 should, in principle, be valid only in the region of $T > 0.5|J|/k_B$ (i.e., ~70 and ~40 K for α-$AgCuPO_4$ and β-$AgCuPO_4$, respectively). For an alternating-chain system, the spin gap for magnetic excitations from the $S = 0$ singlet ground state to the lowest $S = 1$ triplet states is approximately given by [20]

$$\Delta = |J|(1 - \alpha)^{3/4}(1 + \alpha)^{1/4} \quad (7)$$

which leads to $\Delta/k_B = 93.7$ K for α-$AgCuPO_4$ and $\Delta/k_B = 62.3$ K for β-$AgCuPO_4$. In our least-squares fitting analysis of χ_{exp} with the expression of χ_t given by Johnston et al.,[18] we were unable to obtain meaningful results (e.g., see Figure S1 of the Supporting Information). Thus, we did not attempt to calculate the spin gaps using the formulas reported by Johnston et al.[18]

The J/k_B value is greater in magnitude for the low-temperature form α-$AgCuPO_4$ than for the high-temperature form β-$AgCuPO_4$ by a factor of approximately 2 (i.e., −146.1 vs −82.6 K). The ratio of the two exchange parameters, α, is slightly smaller for the high-temperature form than for the low-temperature form (i.e., 0.384 vs 0.519). What is not obvious at this point is if an alternating-chain model is truly appropriate for α- and β-$AgCuPO_4$ in terms of their electronic structures. To answer this question, it is necessary to evaluate the relative strengths of their spin-exchange interactions on the basis of electronic structure calculations. This question is probed in the next section.

6. Spin-Exchange Interactions

Spin-exchange interactions between the Cu^{2+} ions of $AgCuPO_4$ can occur through the superexchange (SE) paths, Cu−O−Cu, or through the super-superexchange (SSE) paths, Cu−O···O−Cu, where the O···O contact forms an edge of the PO_4 group coordinating the two Cu atoms. It is well established that SSE interactions can be strong in magnitude and can be even stronger than SE interactions.[21−24] To determine the spin−lattice structures of α- and β-$AgCuPO_4$, we evaluate the relative strengths of their SE and SSE interactions in terms of spin-dimer analysis based on extended Hückel tight binding (EHTB) calculations.[22−26] The various SE and SSE spin-exchange paths of α- and β-$AgCuPO_4$ are schematically depicted in Figure 7, and the spin dimers associated with these paths are presented in Figure 8 for α-$AgCuPO_4$. In general features, the corresponding spin dimers of β-$AgCuPO_4$ are similar to those of Figure 8 and hence are not shown. The geometrical parameters associated with these spin-exchange paths are summarized in Table 3.

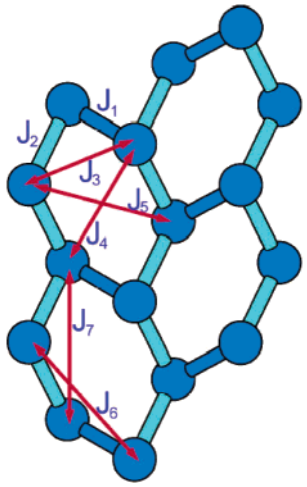

Figure 7. Schematic representation of the seven spin-exchange paths in α- and β-$AgCuPO_4$. As in Figure 4b, each blue cylinder represents a pair of nearest-neighbor Cu atoms linked by two Cu−O−Cu linkages, and each aquamarine cylinder represents a pair linked by one Cu−O−Cu linkage.

Each Cu^{2+} ion of α- and β-$AgCuPO_4$ has one singly occupied d-block orbital (i.e., the magnetic orbital), which is depicted in Figure 9. Consider that the two spin sites of a spin dimer are chemically equivalent, as found for α- and β-$AgCuPO_4$ and that the two magnetic orbitals of a spin dimer interact to result in an energy split, Δe. In the spin-dimer analysis, based on EHTB calculations, the strength of an antiferromagnetic interaction between two spin sites is estimated by considering the antiferromagnetic spin exchange parameter, J_{AF},[22−24]

$$J_{AF} \approx -\frac{(\Delta e)^2}{U_{eff}} \quad (8)$$

where U_{eff} is the effective on-site repulsion that is essentially a constant for a given compound. Thus, the trend in the J_{AF} values is determined by that in the corresponding $(\Delta e)^2$ values. It has been found [22−24] that the magnetic properties of a variety of magnetic solids are well described by the $(\Delta e)^2$ values obtained from EHTB calculations,[25,26] when both the d orbitals of the transition metal and the s/p orbitals of its surrounding ligands are represented by double-ζ Slater-type orbitals.[27] The atomic parameters used for the EHTB calculations of the $(\Delta e)^2$ values are summarized in Table S1 of the Supporting Information. The $(\Delta e)^2$ values and their relative values calculated for the spin-exchange paths J_1−J_7 of α- and β-$AgCuPO_4$ are summarized in Table 4.

Table 4 shows that the SSE path J_4 has the strongest antiferromagnetic interaction in both α- and β-$AgCuPO_4$, and this interaction is stronger for α-$AgCuPO_4$ than for β-$AgCuPO_4$ by a factor of approximately 2. The latter is consistent with the result of our fitting analyses with an alternating-chain model in that the J/k_B value is greater in magnitude for α-$AgCuPO_4$ than for β-$AgCuPO_4$ by a factor of approximately 2 (i.e., −146.1 vs −82.6 K). The structural

(20) Barnes, T.; Riera, J.; Tennant, D. A. *Phys. Rev. B* **1999**, *59*, 11384.
(21) Belik, A. A.; Azuma, M.; Takano, M. *J. Solid State Chem.* **2004**, *177*, 883.
(22) Whangbo, M.-H.; Koo, H.-J.; Dai, D. *J. Solid State Chem.* **2003**, *176*, 417 and references therein.
(23) Whangbo, M.-H.; Dai D.; Koo H.-J. *Solid State Sci.* **2005**, *7*, 827 and references therein.
(24) Koo, H.-J.; Dai, D.; Whangbo, M.-H. *Inorg. Chem.* **2005**, *44*, 4359.
(25) Hoffmann, R. *J. Chem. Phys*. **1963**, *39*, 1397.
(26) Our calculations were carried out with the SAMOA (Structure and Molecular Orbital Analyzer) program package (Dai, D.; Ren, J.; Liang, W.; Whangbo, M.-H. http://chvamw.chem.ncsu.edu, 2002).
(27) Clementi, E.; Roetti, C. *At. Data Nucl. Data Tables* **1974**, *14*, 177.

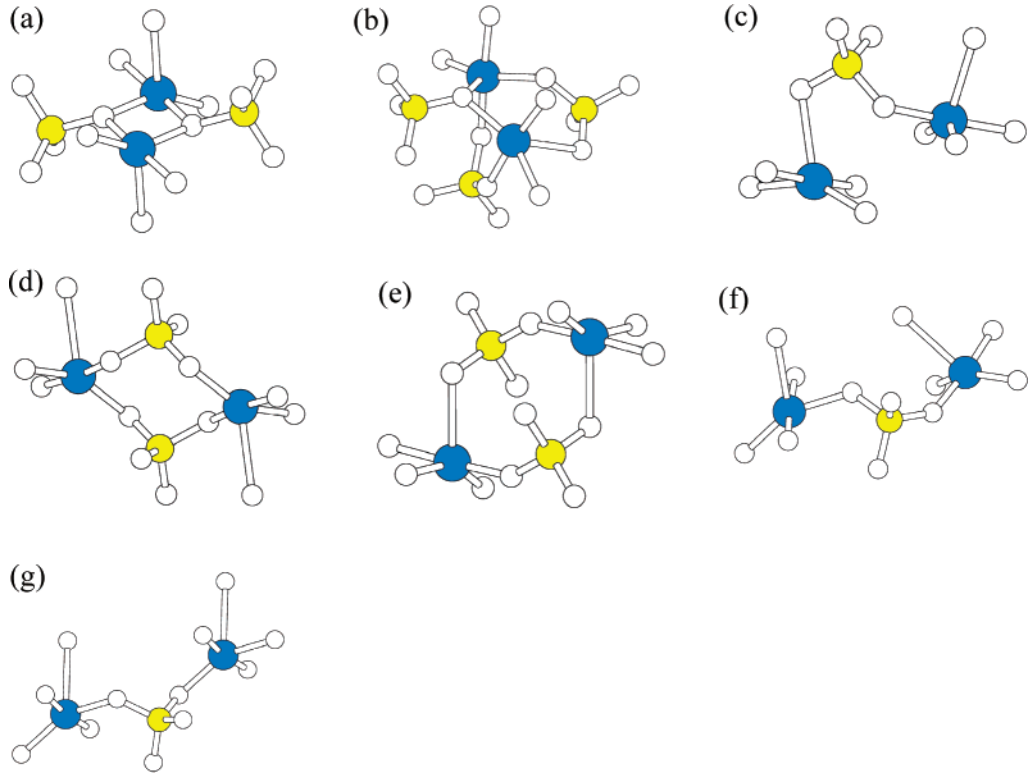

Figure 8. Spin dimers associated with the spin exchange paths J_1-J_7 in β-$AgCuPO_4$, where the blue, yellow, and white circles represent the Cu, P, and O atoms, respectively.

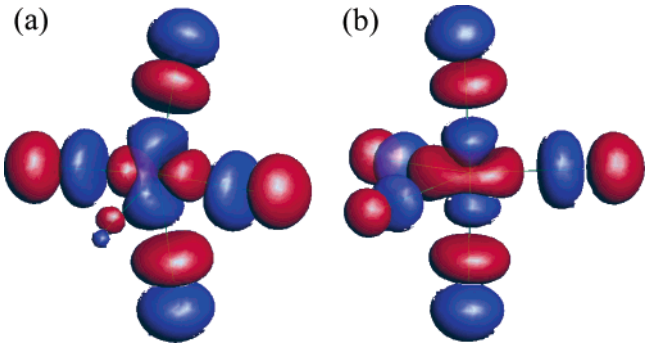

Figure 9. Magnetic orbitals of the spin monomer units CuO_5 in (a) α-$AgCuPO_4$ and (b) β-$AgCuPO_4$.

parameters associated with the J_4 paths (Table 3) show that the O···O contact distance is shorter, and the ∠Cu−O···O angles are greater for α-$AgCuPO_4$ than for β-$AgCuPO_4$. As pointed out elsewhere,[22−24] these two structural factors give rise to a stronger SSE interaction for α-$AgCuPO_4$. In the absence of the PO_4 units, the SSE interaction J_4 becomes negligible. This is an exception to the general observation that for phosphates of Cu^{2+} ions, the relative strengths of the SE and SSE interactions determined by spin-dimer analysis based on EHTB calculations are not strongly affected by the PO_4 tetrahedral units being included in the spin dimers.[22−24,28,29] As described elsewhere,[30] the symmetry of the bridging mode can strongly influence the magnitude of an SSE interaction. In the spin dimer representing SSE interaction J_4 (Figure 8d), the PO_4 units bridge the two Cu^{2+} sites such that the magnetic orbitals of both Cu^{2+} sites can overlap well with one π-type group orbital of each PO_4 unit. This makes the J_4 interaction strong.

The second-strongest antiferromagnetic interaction in β-$AgCuPO_4$ is the SE interaction J_1, while the remaining interactions are weaker. Thus, as depicted in Figure 10a, the two strongest interactions, J_4 and J_1, of β-$AgCuPO_4$ form alternating chains. This is in support of the use of an alternating-chain model for describing the magnetic structure of β-$AgCuPO_4$. The J_1/J_4 ratio is 0.17, which is considerably smaller than the α value (i.e., 0.519) obtained from the fitting analysis. This discrepancy may have resulted in part from the fact that the alternating chains defined by J_4 and J_1 are not truly isolated as assumed in the fitting analysis but interact through other weaker exchange paths (e.g., J_5 and J_6).

The second-strongest antiferromagnetic interaction in α-$AgCuPO_4$ is the SE interaction J_2, while the remaining interactions are weaker. Thus, as depicted in Figure 10b, the two strongest interactions, J_4 and J_2, of α-$AgCuPO_4$ form a two-dimensional net. Therefore, it is not quite correct to describe the magnetic susceptibility of α-$AgCuPO_4$ in terms of an alternating-chain model, although its use leads to an excellent fitting. Nevertheless, the two-dimensional net of Figure 10b can be broken into a set of alternating chains defined by the paths J_4 and J_2, and such chains interact via

(28) Koo, H.-J.; Whangbo, M.-H.; VerNooy, P. D.; Torardi, C. C.; Marshall, W. J. *Inorg. Chem.* **2002**, *41*, 4664.
(29) Belik, A. A.; Azuma, M.; Matsuo, A.; Whangbo, M.-H.; Koo, H.-J.; Kikuchi, J.; Kaji, T.; Okubo, S.; Ohta, H.; Kindo, K.; Takano, M. *Inorg. Chem.* **2005**, *44*, 6632.
(30) Koo, H.-J.; Whangbo, M.-H. *Inorg. Chem.* **2006**, *45*, 4440.
(31) Brese, N. E.; O'Keefe, M. *Acta Crystallogr.* **1991**, *B47*, 192.

Table 3. Values of the Geometrical Parameters for Various Spin-Exchange Paths in α-$AgCuPO_4$ and β-$AgCuPO_4$[a]

path	α-$AgCuPO_4$	β-$AgCuPO_4$
J_1	Cu···Cu = 3.05	Cu···Cu = 3.10
	Cu−O−Cu (×2) Cu−O = 1.92, 2.02 ∠Cu−O−Cu = 101.2	Cu−O−Cu (×2) Cu−O = 1.93, 2.20 ∠Cu−O−Cu = 93.9
J_2	Cu···Cu = 3.37	Cu···Cu = 3.37
	Cu−O−Cu Cu−O = 2.03, 2.59 ∠Cu−O−Cu = 93.3	Cu−O−Cu Cu−O = 2.14, 1.96 ∠Cu−O−Cu = 102.4
	Cu−O···O−Cu Cu−O = 2.02, 2.59 O···O = 2.443 ∠Cu−O···O = 67.6, 119.0	Cu−O···O−Cu Cu−O = 2.20, 2.14 O···O = 2.556 ∠Cu−O···O = 109.2, 80.7
	Cu−O···O−Cu Cu−O = 1.92, 1.88 O···O = 2.55 ∠Cu−O···O = 92.1, 111.4	Cu−O···O−Cu: Cu−O = 1.94, 1.93 O···O = 2.45 ∠Cu−O···O = 104.3, 96.9
J_3	Cu···Cu = 4.02	Cu···Cu = 4.05
	Cu−O···O−Cu Cu−O = 1.92, 2.59 O···O = 2.44 ∠Cu−O···O = 137.8, 67.6	Cu−O···O−Cu Cu−O = 1.93, 2.14 O···O = 2.56 ∠Cu−O···O = 124.1, 80.7
J_4	Cu···Cu = 5.07	Cu···Cu = 5.20
	Cu−O···O−Cu (×2) Cu−O = 1.92, 2.03 O···O = 2.44 ∠Cu−O···O = 137.8, 125.3	Cu−O···O−Cu (×2) Cu−O = 1.96, 1.93 O···O = 2.56 ∠Cu−O···O = 121.7, 130.4
J_5	Cu···Cu = 5.42	Cu···Cu = 5.12
	Cu−O···O−Cu (×2) Cu−O = 2.59, 1.88 O···O = 2.51 ∠Cu−O···O = 121.7, 130.4	Cu−O···O−Cu (×2) Cu−O = 1.94, 2.14 O···O = 2.56 ∠Cu−O···O = 115.8, 132.2
J_6	Cu···Cu = 5.61	Cu···Cu = 5.61
	Cu−O···O−Cu Cu−O = 1.88, 2.02 O···O = 2.55 ∠Cu−O···O = 111.4, 148.9	Cu−O···O−Cu Cu−O = 1.94, 2.20 O···O = 2.45 ∠Cu−O···O = 104.3, 166.1
J_7	Cu···Cu = 5.63	Cu···Cu = 5.70
	Cu−O···O−Cu Cu−O = 2.02, 2.03 O···O = 2.44 ∠Cu−O···O = 119.0, 125.3	Cu−O···O−Cu Cu−O = 2.20, 1.96 O···O = 2.56 ∠Cu−O···O = 109.2, 141.1

[a] Bond lengths in angstroms and bond angles in degrees.

Table 4. Calculated $(\Delta e)^2$ Values for Various Spin-Exchange Paths in α-$AgCuPO_4$ and β-$AgCuPO_4$[a]

path	α-$AgCuPO_4$		β-$AgCuPO_4$	
J_1	190	(0.01)	1700	(0.17)
J_2	4200	(0.20)	640	(0.06)
J_3	85	(0.00)	770	(0.08)
J_4	21000	(1.00)	10000	(1.00)
J_5	310	(0.02)	1200	(0.12)
J_6	25	(0.00)	910	(0.09)
J_7	1100	(0.05)	120	(0.01)

[a] The $(\Delta e)^2$ values are in millielectronvolts squared, and the relative values are given in parentheses.

the J_2 paths. This might explain why the magnetic susceptibility of α-$AgCuPO_4$ can be well simulated with an alternating-chain model and why the J_2/J_4 ratio (i.e., 0.20) is smaller than the α value (i.e., 0.384) obtained from the fitting analysis.

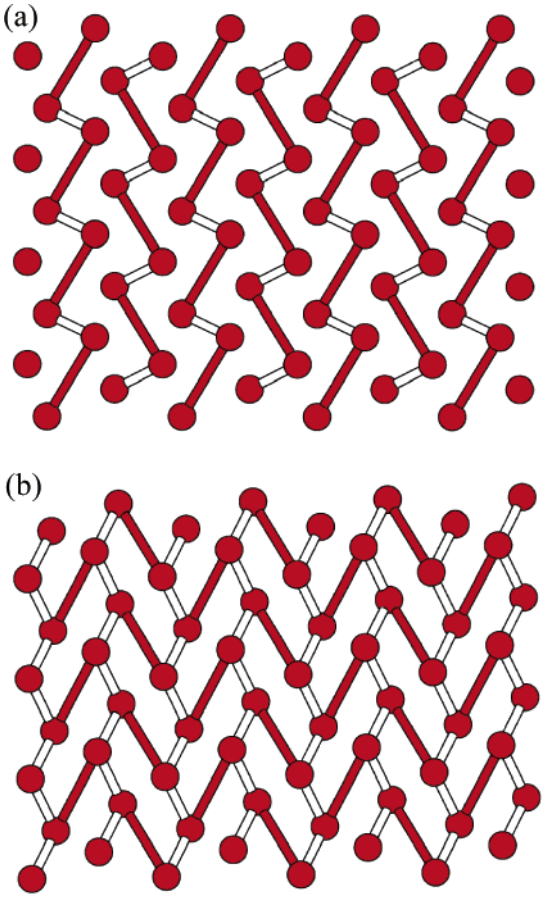

Figure 10. Spin lattices of (a) β-$AgCuPO_4$ and (b) α-$AgCuPO_4$ that are defined by their two strongest spin-exchange paths. For both α- and β-$AgCuPO_4$, the strongest and second-strongest spin-exchange interaction paths are represented by red and white cylinders, respectively.

7. Concluding Remarks

The low-temperature form of $AgCuPO_4$ (i.e., α-$AgCuPO_4$) is similar in crystal structure to that of the high-temperature form (i.e., β-$AgCuPO_4$) in that they both have $Cu_2P_2O_8$ layers alternating with silver-atom double layers. In α-$AgCuPO_4$, the arrangement of the Cu and P atoms in all the $Cu_2P_2O_8$ layers has the same spatial orientation so that a unit cell has one $Cu_2P_2O_8$ layer. In β-$AgCuPO_4$, the arrangements of the Cu and P atoms in two adjacent $Cu_2P_2O_8$ layers have two different spatial orientations so that a unit cell has two $Cu_2P_2O_8$ layers. The two forms of $AgCuPO_4$ differ in the local coordinate environments of their Cu^{2+} ions; the coordinate environment of each Cu^{2+} ion is close to a distorted square pyramid in α-$AgCuPO_4$ and to a distorted trigonal pyramid in β-$AgCuPO_4$. The magnetic susceptibilities of α- and β-$AgCuPO_4$ show a maximum at ∼75 and ∼50 K, respectively, and are well simulated by an antiferromagnetic alternating-chain model, which leads to $J/k_B = -146.1$ K, $\alpha J/k_B = -75.8$ K, and $\Delta/k_B = 93.7$ K for α-$AgCuPO_4$ and $J/k_B = -82.6$ K, $\alpha J/k_B = -31.7$ K, and $\Delta/k_B = 62.3$ K for β-$AgCuPO_4$. The strongest spin exchange in both forms of $AgCuPO_4$ comes from the SSE path J_4, and this interaction is stronger for α-$AgCuPO_4$ than for β-$AgCuPO_4$ by a factor of ∼2, in good agreement with the experiment. Our analysis supports the use of this model for

β-$AgCuPO_4$ and predicts that the spin lattice of α-$AgCuPO_4$ should be better described by a two-dimensional net composed of weakly interacting alternating chains. This difference between the spin lattices of the two forms of $AgCuPO_4$ originates from the slight difference in the coordinate environments of their Cu^{2+} ions.

Acknowledgment. The work at NCSU was supported by the Office of Basic Energy Sciences, Division of Materials Sciences, U.S. Department of Energy, under Grant DE-FG02-86ER45259.

Supporting Information Available: Crystallographic data of α-$AgCuPO_4$ in CIF format, a figure showing χ_{mol} vs T plots, and tables of fitting parameters and ζ_i, H_{ii}, and χ_i for the extended Hückel tight binding calculations. This material is available free of charge via the Internet at http://pubs.acs.org.

IC060484L